General theory for calculating disorder-averaged Green's function correlators within the coherent potential approximation

Chenyi Zhou* and Hong Guo

Center for the Physics of Materials and Department of Physics, McGill University, Montreal, H3A 2T8, Canada

(Received 20 November 2016; revised manuscript received 28 December 2016; published 17 January 2017)

We report a diagrammatic method to solve the general problem of calculating configurationally averaged Green's function correlators that appear in quantum transport theory for nanostructures containing disorder. The theory treats both equilibrium and nonequilibrium quantum statistics on an equal footing. Since random impurity scattering is a problem that cannot be solved exactly in a perturbative approach, we combine our diagrammatic method with the coherent potential approximation (CPA) so that a reliable closed-form solution can be obtained. Our theory not only ensures the internal consistency of the diagrams derived at different levels of the correlators but also satisfies a set of Ward-like identities that corroborate the conserving consistency of transport calculations within the formalism. The theory is applied to calculate the quantum transport properties such as average ac conductance and transmission moments of a disordered tight-binding model, and results are numerically verified to high precision by comparing to the exact solutions obtained from enumerating all possible disorder configurations. Our formalism can be employed to predict transport properties of a wide variety of physical systems where disorder scattering is important.

DOI: 10.1103/PhysRevB.95.035126

I. INTRODUCTION

With the down scaling of semiconductor technology and the constant discovery of emerging electronic materials and device concepts [1], electronic device physics is facing new realities and challenges. A particularly important issue is how to approach quantum transport in the nanometer regime [2,3], where detailed atomistic information of the device structure is required for both qualitative and quantitative predictions. In particular, disorder effects can have significant influence on transport properties of electronic nanostructures. In practical materials, disorder includes impurities, surface and interface roughness, grain boundary, material inhomogeneity, etc.. These imperfections of the material cause disorder scattering of charge carriers that result in fluctuations in the measured transport data. In transistor design, random dopant position in the transistor channel gives rise to the phenomenon of device-to-device variability, which severely reduces the reliability of the resulting circuit, a problem that must be controlled in nanoelectronics [4–6].

Theoretically, it is extremely demanding to formulate a first principles formalism for quantum and atomistic device simulation in the presence of random impurities. While solving the quantum transport problem for a single microscopic configuration of random imperfections is now possible from atomic first principles [7], for nanostructures containing disorder such calculations are insufficient: A statistical approach that averages over an ensemble of atomic configurations is necessary for revealing the intrinsic physics and for predicting the general trend of quantum transport. The central quantity in the Green's function formalism that is most relevant to this topic is the configurationally averaged correlator

$$L^{(n)}(\{p,p',X_p\}) \equiv \langle \mathcal{G}^{X_1}(1,1')\ldots\mathcal{G}^{X_n}(n,n')\rangle_{\{v_i\}}, \qquad (1)$$

where 1, p, and n are space-time variables, $\mathcal{G}$ denotes the Green's function under a specified disorder potential profile $\{v_i\}$, and $X = \{\text{retarded } (R), \text{advanced } (A), \text{Keldysh } (K)\}$ denotes the specific type of the real-time Green's function [8,9]. Note that as the Keldysh component of the Green's function has been included in Eq. (1), the correlators can incorporate quantum statistical information of transport far from equilibrium. The quantity (1) is of general interest since many quantum transport properties can be expressed in terms of it. For instance, linear response conductivity [10–12] and quantum transmission coefficient [2,13] are associated with $L^{(2)}$, nonlinear conductance and Hall coefficient [14,15] can be related to $L^{(3)}$, conductance fluctuation [5,16–19] and shot noise [20–22] can be expressed with $L^{(4)}$, etc.

The simple and direct way to evaluate quantity (1) is to sample a sufficiently large number of microscopic atomic configurations, perform Green's function calculations on each of them, and then average over the products. Such a brute-force averaging, apart from being theoretically inelegant, suffers from several problems. For instance, as the translational symmetry of a periodic structure is broken in the presence of random impurities, one needs a large supercell in order to mimic a realistic disorder environment. In addition, when the impurity concentration is small, which is often the case in semiconductors, e.g., $x \sim 0.1\%$, 10 000 atomic sites are needed to just accommodate 10 disordered sites and, with the resulting huge configurational ensemble, such calculation is not possible from first principles even using modern supercomputers.

Therefore, to predict disorder effects in nanostructures from quantum first principles, it is necessary to develop a theoretical formalism to directly evaluate quantity (1) without relying on the brute-force sampling of enormous disorder ensembles. In this regard, the most commonly applied theoretical formalism is the coherent potential approximation (CPA) [23]. Ever since the pioneer work of Soven [24] and Taylor [25], the CPA formalism has been developed to be able to handle all Green's function correlators up to $L^{(2)}$ in both linear response [11,26] and the far-from-equilibrium regime [13,20,27–29].

*chenyi.zhou@mail.mcgill.ca

Atomistic implementations from first principles in conjunction with CPA have also been developed and used to make accurate predictions for a variety of nanoelectronic structures even at relatively high impurity concentrations [13,26,30–35].

Despite its practical success, there are still unsolved theoretical issues remaining in the current CPA formalism. First of all, to the best of our knowledge all existing CPA theories on the $L^{(2)}$ level rely on the so-called single-site decoupling approximation (SSA) [11,13,20], which seems an additional approximation on top of CPA. Although SSA is fully consistent with the single-particle CPA Green's functions as demonstrated in Refs. [23,27,28], it is not obvious whether SSA is necessary or fully compatible in the CPA calculation of $L^{(2)}$ correlators in the Keldysh formalism [20]. Based on a diagrammatic extension of SSA, attempts to formulate a CPA theory for $L^{(3)}$ and $L^{(4)}$ correlators were made by Levin *et al.* [14] and Zhu *et al.* [5] respectively. However, for these higher order correlators, the compatibility of SSA with CPA turns out to be unclear and could even lead to unphysical results at relatively high impurity concentrations, as shown numerically in Ref. [5]. Finally, it is so far not clear how to evaluate the $L^{(3),(4)}$ correlators when $\mathcal{G}^K$ is involved.

To solve these important theoretical issues and to push the frontier of quantum transport theory for disordered nanostructures, in this paper we report a unified diagrammatic theory for consistently evaluating the quantity (1) under CPA. The internal consistency of our theory is guaranteed by the requirement that all the diagrammatic building blocks be derived from the basic CPA single-particle self-energy and therefore no other approximations such as SSA are needed. In addition, we show that our diagrammatic approach displays conserving properties on all levels so that it is especially well suited for quantum transport calculations.

The rest of this paper is organized as follows. In Sec. II, by means of the functional derivative technique, we derive the consistent diagrammatic approach to the general disorder-averaging problem defined in Eq. (1) and then demonstrate how the diagrammatic method is implemented in conjunction with CPA. In Sec. III, the theory is applied to a tight-binding numerical model of a two-probe transport junction to demonstrate its usage. Higher order moments of transmission probability distribution due to random disorder are calculated and the predictions are compared with the exact results obtained from the brute-force calculation of all possible disorder configurations. We also employ our method to investigate the disorder-averaged dynamic conductance under ac bias, where we find that charge conservation is ensured thanks to the internal consistency of our theory. Finally, some technical details about the diagrams and further mathematical analysis regarding the consistency of our theory are provided in the appendices.

II. THEORETICAL METHOD

A. General theory of disorder averaging

We consider in this paper the model of noninteracting electrons subjected to a random diagonal disorder potential, which is described by the Hamiltonian

$$H = \sum_{ij} \theta_{ij} a_i^\dagger a_j + \sum_i v_i a_i^\dagger a_i,$$

where θ_{ij} is the disorder-independent hopping matrix and $a_i^\dagger$ (a_i) is the creation (annihilation) operator for an electron on site i. The disorder is modeled by the onsite energy v_i, which is a site-dependent random variable.

To derive the diagrammatic scheme for calculating $L^{(n)}$ of Eq. (1), we shall utilize the functional derivative method adapted from Ref. [36] and apply it in the Keldysh path-integral formalism [9]. The basics of the Keldysh path-integral formalism relevant to our methodology are provided in Appendix A. We start with the definition of the generalized configurationally averaged n-particle Green's function [8,9,36–40]:

$$\begin{aligned} &G^{(n)}(1,\ldots,n;1',\ldots,n';U) \\ &\quad\equiv \frac{1}{i^n}\langle\psi(1)\ldots\psi(n)\bar{\psi}(n')\ldots\bar{\psi}(1')\rangle_{S[U]} \\ &\quad= \frac{1}{i^n}\frac{\int D[\psi,\bar{\psi}]e^{iS}\psi(1)\ldots\psi(n)\bar{\psi}(n')\ldots\bar{\psi}(1')}{\int D[\psi,\bar{\psi}]e^{iS}}, \end{aligned} \tag{2}$$

where ψ and $\bar{\psi}$ are the fermionic Grassmann variable and its conjugate [9]. The collective index is understood as $1 \equiv \{i_1,t_1,k_1\}$, where i denotes an atomic site, t is a real-time variable, and k denotes a Keldysh component which takes either "cl" (classical) or "q" (quantum) [9]. The total action is defined as $S = S_0 - S_U - S_\mathrm{d}$, where S_0 and S_d are defined in Eqs. (A5), (A2), and (A6) in terms of the cl/q-field components. The auxiliary source field U, which will be taken as zero at the end, enters the action via

$$S_U = \int d1d2\bar{\psi}(1)U(1,2)\psi(2).$$

Since S_d contains nonquadratic terms, in order to approach $G^{(n)}$ we expand e^{-iS_d} in its Taylor series and, with the aid of Wick's theorem [9,38], $G^{(n)}$ is then expressed with a series of Feymann diagrams, which can be constructed according to the standard procedure: Each kth-order diagram consists of k interaction vertices, $2n$ external legs labeled by $1,\ldots,n,1',\ldots,n'$, and a topologically distinct connection between all vertices and legs with directed Green's function lines [8,9,38,39].

Particularly, for the generalized single-particle Green's function we have the following Dyson equation preserved in its regular form [8,36]:

$$G^{-1}(11',U) = G_0^{-1}(11') - U(11') - \tilde{\Sigma}(11',U). \tag{3}$$

Here we use $\tilde{\Sigma}$ to denote the full set of self-energy diagrams including the ones containing internal loops [see Fig. 1(b)]. These loop-containing diagrams all vanish at the end upon taking $U \to 0$ because each loop then induces a factor of the form $[G^R(t,t) + G^A(t,t)]$, which equals zero by construction of the Keldysh formalism [9]. However, note that these diagrams should be taken into account along our derivation in order to get correct diagrams for higher order correlators. Later, Σ will be used to denote the part of $\tilde{\Sigma}$ with all loop-containing diagrams excluded, i.e., the actual self-energy for the disorder scattering problem [9,39] [see the illustration in Fig. 1(a)].

The central quantities of our interest are the real-time single-particle Green's functions [9] defined in Eq. (A4) and the nth-order correlator [see Eq. (1)], which can be expressed

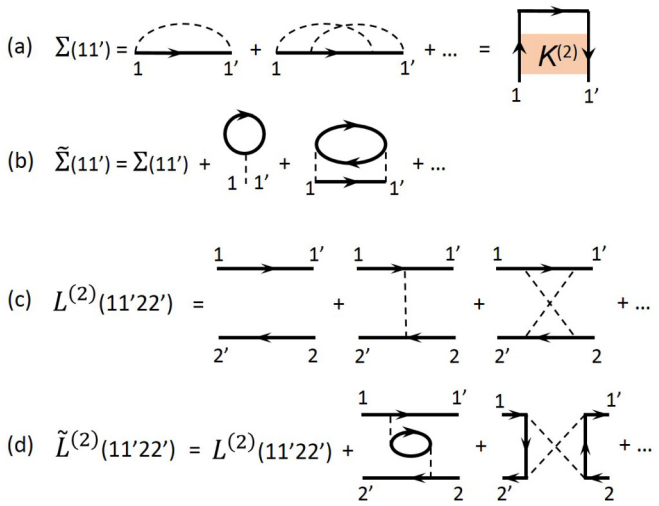

FIG. 1. Diagrammatic visualization of self-energies Σ, $\tilde{\Sigma}$ and correlators $L^{(2)}$, $\tilde{L}^{(2)}$. The directed thick line represents the average Green's function. Dashed lines represent disorder vertices.

with the Grassmann algebra as

$$L^{(n)}(11',\ldots,nn') = \frac{1}{i^n}\langle\widehat{\psi(1)\bar{\psi}(1')}\ldots\widehat{\psi(n)\bar{\psi}(n')}\rangle_{S[U\to 0]}. \tag{4}$$

Here we use the hat notation to emphasize a particular pairing of the external Grassmann variables: In the diagrammatic language, only those diagrams with every external leg (e.g., m) connected to its counterpart (e.g., m') via Green's functions (represented by directed lines) make nonzero contributions to $L^{(n)}$. Therefore, $L^{(n)}$ can be viewed as a particular part of $G^{(n)}$ with a restricted diagram topology.

In principle, all the diagrams of $G^{(n)}$, and hence those of $L^{(n)}$, can be enumerated according to the diagram rule. However, apart from being inefficient, such brute-force approach does not provide much insight into the internal relation between the Green's function correlators and is thus not very useful for deriving our consistent scheme of calculating $L^{(n)}$. In contrast, we find the functional derivative technique to be a suitable method for our purpose.

From the definition Eq. (2) it can be seen that $G^{(n+1)}[U]$ is associated with the nth-order derivative of $G[U]$ with respect to U [36]. For example, the first-order derivative yields

$$\begin{aligned}\frac{\delta G(12')}{\delta U(1'2)} &= G^{(2)}(12;1'2') + G(12')G(21')\\ &\equiv \tilde{L}^{(2)}(11',22'),\end{aligned} \tag{5}$$

where an auxiliary quantity $\tilde{L}^{(2)}$ has been introduced. Similar to the Dyson equation, $\tilde{L}^{(2)}$ satisfies a recursive relation, namely the Bethe-Salpeter equation [36,37,39] (repeated indices are assumed to be integrated over):

$$\begin{aligned}\tilde{L}^{(2)}(11'22') &= G(11')G(22') + G(1\bar{3})G(\bar{4}2')\tilde{K}^{(2)}\\ &\quad\times(\bar{3}\bar{6}\bar{5}\bar{4})\tilde{L}^{(2)}(\bar{6}1'2\bar{5}).\end{aligned} \tag{6}$$

The kernel is defined as $\tilde{K}^{(2)}(\bar{3}\bar{6}\bar{5}\bar{4}) \equiv \delta\tilde{\Sigma}(\bar{3}\bar{4})/\delta G(\bar{6}\bar{5})$, where the functional derivative means removing one Green's function line from each of the $\tilde{\Sigma}$ diagrams [37]. The derivation for

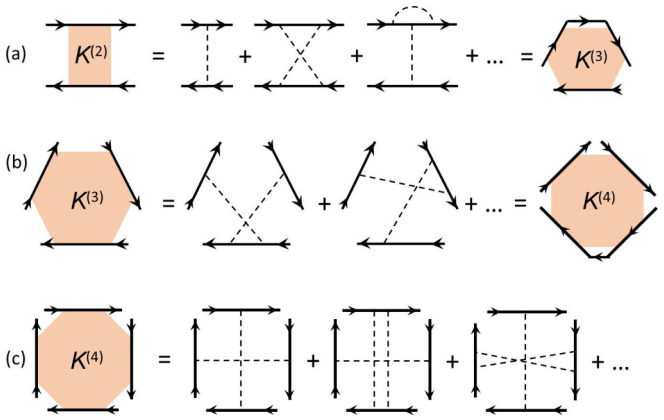

FIG. 2. Diagrammatic illustration of high-order kernels and their relations. Dashed lines represent disorder vertices.

Eq. (6) is analogous to the one presented in Ref. [36] except that here each collective index contains a Keldysh component in addition to the space-time variable. Diagrams of $\tilde{L}^{(2)}$ can be generated according to Eq. (6) and we provide some of the examples in Fig. 1. As can be seen, $\tilde{L}^{(2)}$ involves diagrams of both the horizontal channel, where 1, 2 are connected to $1',2'$ respectively, and the vertical channel where 1, 2 are connected to $2',1'$ respectively; diagrams of the latter type are irrelevant to $L^{(2)}$ [see Eq. (4)]. Besides, all the loop-containing $\tilde{L}^{(2)}$ diagrams should vanish at the end [9,39]. All these noncontributing diagrams can be excluded by keeping those kernel diagrams derived from Σ only, that is, using $K^{(2)} \equiv \delta\Sigma/\delta G$ [see Figs. 1(a) and 2(a)] to replace $\tilde{K}^{(2)}$ in the Bethe-Salpeter equation:

$$\begin{aligned}L^{(2)}(11'22') &= G(11')G(22') + G(1\bar{3})G(\bar{4}2')K^{(2)}\\ &\quad\times(\bar{3}\bar{6}\bar{5}\bar{4})L^{(2)}(\bar{6}1'2\bar{5}).\end{aligned} \tag{7}$$

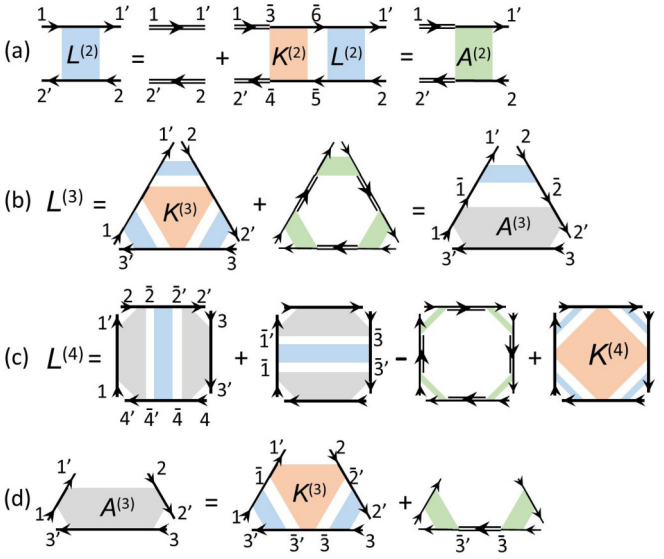

FIG. 3. Diagrammatic visualization of the correlators $L^{(2)}$, $L^{(3)}$, $L^{(4)}$, and auxiliary functions $A^{(2)}$ and $A^{(3)}$. Directed double lines represent the average Green's function. The same diagrammatic building blocks are marked by same colors. Internal indices are to be integrated over.

To simplify the notations we introduce the symbols $\bullet$ for direct product operations, $\odot$ for inner product operations, and $\overleftarrow{G}$ ($\overrightarrow{G}$) for the left-going (right-going) Green's function lines in the diagrams of Figs. 1(c) and 1(d), so that Eq. (7) can be rewritten as

$$L^{(2)} = \left(\begin{matrix}\overrightarrow{G}\\ \bullet \\ \overleftarrow{G}\end{matrix}\right) + \left(\begin{matrix}\overrightarrow{G}\\ \bullet \\ \overleftarrow{G}\end{matrix}\right) \odot K^{(2)} \odot L^{(2)}. \tag{8}$$

The interpretation of such algebraic expression should be clear according to its diagrammatic representation in Fig. 3(a).

Next, we look to derive the diagrams for $L^{(3)}$. Since $L^{(3)}$ is embraced by $G^{(3)}$ and $G^{(3)}$ is in turn associated with $\delta^2 G/\delta U^2$, we differentiate both sides of Eq. (6) with respect to U:

$$\begin{aligned}
\frac{\delta \tilde{L}^{(2)}}{\delta U} &= \frac{\delta}{\delta U}\left[\left(\begin{matrix}\overrightarrow{G}\\ \bullet \\ \overleftarrow{G}\end{matrix}\right) + \left(\begin{matrix}\overrightarrow{G}\\ \bullet \\ \overleftarrow{G}\end{matrix}\right) \odot \tilde{K}^{(2)} \odot \left(\begin{matrix}\overrightarrow{G}\\ \bullet \\ \overleftarrow{G}\end{matrix}\right) + \cdots\right] \\
&= \cdots + \left[\cdots \tilde{K}^{(2)} \odot \left(\begin{matrix}\overrightarrow{G}\\ \bullet \\ \overleftarrow{\delta G/\delta U}\end{matrix}\right) \odot \tilde{K}^{(2)} \odot \cdots\right] \\
&\quad + \left[\cdots \tilde{K}^{(2)} \odot \left(\begin{matrix}\overrightarrow{\delta G/\delta U}\\ \bullet \\ \overleftarrow{G}\end{matrix}\right) \odot \tilde{K}^{(2)} \odot \cdots\right] \\
&\quad + \left[\cdots \tilde{K}^{(2)} \odot \left(\begin{matrix}\overrightarrow{G}\\ \bullet \\ \overleftarrow{G}\end{matrix}\right) \odot \frac{\delta \tilde{K}^{(2)}}{\delta U} \odot \cdots\right] + \cdots \\
&= \cdots + \left[\cdots \tilde{K}^{(2)} \odot \left(\begin{matrix}\overrightarrow{G}\\ \bullet \\ \tilde{L}^{(2)}\end{matrix}\right) \odot \tilde{K}^{(2)} \odot \cdots\right] \\
&\quad + \left[\cdots \tilde{K}^{(2)} \odot \left(\begin{matrix}\tilde{L}^{(2)}\\ \bullet \\ \overleftarrow{G}\end{matrix}\right) \odot \tilde{K}^{(2)} \odot \cdots\right] \\
&\quad + \left[\cdots \tilde{K}^{(2)} \odot \left(\begin{matrix}\overrightarrow{G}\\ \bullet \\ \overleftarrow{G}\end{matrix}\right) \odot \left(\begin{matrix}\tilde{L}^{(2)}\\ \odot \\ \tilde{K}^{(3)}\end{matrix}\right) \odot \cdots\right] + \cdots,
\end{aligned} \tag{9}$$

where we have used Eq. (5) and the chain rule $\delta \tilde{K}^{(2)}/\delta U = [\delta \tilde{K}^{(2)}/\delta G] \odot [\delta G/\delta U] = \tilde{K}^{(3)} \odot \tilde{L}^{(2)}$. Again Eq. (9) involves diagrams with all kinds of external leg pairings; filtering out irrelevant terms, we arrive at

$$\begin{aligned}
L^{(3)} &= \cdots + \left[\cdots \left(\begin{matrix}\overrightarrow{G}\\ \bullet \\ \overleftarrow{G}\end{matrix}\right) \odot K^{(2)} \odot \left(\begin{matrix}L^{(2)}\\ \bullet \\ \overleftarrow{G}\end{matrix}\right) \odot K^{(2)} \odot \cdots\right] \\
&\quad + \left[\cdots K^{(2)} \odot \left(\begin{matrix}\overrightarrow{G}\\ \bullet \\ \overleftarrow{G}\end{matrix}\right) \odot \left(\begin{matrix}L^{(2)}\\ \odot \\ K^{(3)}\end{matrix}\right) \odot \left(\begin{matrix}\overrightarrow{G}\\ \bullet \\ \overleftarrow{G}\end{matrix}\right) \odot \cdots\right] + \cdots \\
&= A^{(2)} \odot \left(\begin{matrix}L^{(2)}\\ \bullet \\ \overleftarrow{G}\end{matrix}\right) \odot A^{(2)} + L^{(2)} \odot \left(\begin{matrix}L^{(2)}\\ \odot \\ K^{(3)}\end{matrix}\right) \odot L^{(2)}.
\end{aligned} \tag{10}$$

where $A^{(2)} \equiv 1 \bullet 1 + K^{(2)} \odot L^{(2)}$ [see Fig. 3(a) and Eq. (B2)] and $K^{(3)}[G] \equiv \delta K^{(2)}/\delta \overrightarrow{G}$ (see Fig. 2). The diagrammatic visualization of Eq. (10) is shown in Fig. 3(b) and its explicit expression is given by Eq. (B3) in Appendix B. In principle one can continue to generate the diagrams of $L^{(4)}$, $L^{(5)}$, and so forth. Although the higher-order diagrams become more complex, the generating procedure remains tractable with the functional derivative method. As the final example, $L^{(4)}$ is given by Fig. 3(c) and Eq. (B4), with examples of $K^{(4)}$ provided in Fig. 2(c).

One central observation from the functional derivative approach is that the building blocks of all the $L^{(n)}$ diagrams, i.e., the kernels $K^{(n)}$, are derived from the single-particle self-energy diagrams by successively removing Green's function lines [41]:

$$K^{(n+1)}[G] = \frac{\delta^n \Sigma}{\delta G^n}. \tag{11}$$

Consequently, in principle if one could obtain the analytical expression of $\Sigma[G]$ or could enumerate all the Σ diagrams, the correlators $L^{(n)}$ would hence be solved exactly with the diagrammatic scheme of Fig. 3. Unfortunately this is generally impractical and therefore one has to approximate $K^{(n)}$ using certain subset of diagrams according to specific physical concerns or accuracy demands. Naively, one may consider that as one takes into account more diagrams, the results are the more accurate. This consideration may or may not be valid depending on whether the elaborated approximations at different diagrammatic levels preserve some consistency. Here the consistency is considered from two aspects. First, if a quantity can be evaluated by diagrams on different levels of $L^{(n)}$ within the same framework, same result should be obtained at the end regardless of what diagrams are actually used; we refer to this as the interlevel consistency. For example, the disorder-averaged dc shot noise of a two-probe transport junction can be expressed either with $L^{(2)}$ or with $L^{(4)}$ [5,20]; thus a consistent diagrammatic method should yield the same final result for the shot noise (a physical quantity) regardless of which $L^{(n)}$ was actually used in middle steps of the derivation. This point will be further illustrated in Sec. III below. The second consistency is whether the averaged transport properties calculated by the diagrammatic method can meet the basic conservation requirements [11,12,36,42–45], which we refer to as the conservation consistency. The conservation consistency is usually associated with the Ward identity [11,12,43–45]. These consistency requirements lead to constraints on the choice of $K^{(n)}$ diagrams. To elucidate such constraints we hereby propose a unified approximation scheme, which we call the Σ-derivable theory, for all the $K^{(n)}$ diagrams: Namely we require that all kernels be derived from the approximated self-energy in the way suggested by Eq. (11) once the approximation method for the latter has been specified. The interlevel consistency of Σ-derivable theory is verified in Sec. III by examining a two-probe transport junction. In terms of conservation consistency, we find that our theory satisfies a group of Ward-type identities, to be presented in Sec. II B. In addition, the Σ-derivable theory can be shown to be consistent with the nonequilibrium vertex correction (NVC) theory under CPA [13,20] (see Appendix D), which is by far the most accurate two-particle CPA theory for nonequilibrium quantum transport. We conclude that the Σ-derivable scheme amounts to the consistent approximation method that we are looking for.

B. Ward-type identities

If the system is in a steady state, all the quantities can be transformed into frequency domain by means of Fourier transform with respect to the time difference $(t - t')$ [3]. In

this case, we have

$$\mathcal{G}^{R/A}(\omega) = \left\{\left[G_0^{R/A}(\omega)\right]^{-1} - V\right\}^{-1} = \{[G_0(z^{\pm})]^{-1} - V\}^{-1} \equiv \mathcal{G}(z^{\pm}), \quad (12)$$

where $z^{\pm} = \omega \pm i0^{+}$ is the complex frequency [12] and V denotes the potential profile of a particular disorder configuration. From Eq. (12) we obtain the following identity:

$$\mathcal{G}_{ij}(z_1)C_{jk}(z_1,z_2)\mathcal{G}_{kl}(z_2) = \mathcal{G}_{il}(z_1) - \mathcal{G}_{il}(z_2),$$

where $C(z_1,z_2) \equiv [G_0(z_2)]^{-1} - [G_0(z_1)]^{-1}$ and the Latin letters in subscripts denote the matrix elements in real-space basis (repeated indices are assumed to be summed over). Taking configurational average on both sides, we get

$$\langle \mathcal{G}_{ij}(z_1)C_{jk}(z_1,z_2)\mathcal{G}_{kl}(z_2)\rangle = G_{il}(z_1) - G_{il}(z_2). \quad (13)$$

Note that this identity is not trivial because the right-hand side consists of single-particle Green's functions only while the left-hand side is associated with $L^{(2)}$. Equation (13) is known as the Velický's version of Ward identity [11], which is viewed as a consistent relation between G and $L^{(2)}$.

Similarly, we can generate other Ward-type identities:

$$\begin{aligned}&\left\langle \mathcal{G}_{ij}(z_1)C_{jk}(z_1,z_2)\mathcal{G}_{kl}(z_2)\mathcal{G}_{p_3p_3'}(z_3)\ldots\mathcal{G}_{p_np_n'}(z_n)\right\rangle \\ &\quad = \left\langle \mathcal{G}_{il}(z_1)\mathcal{G}_{p_3p_3'}(z_3)\ldots\mathcal{G}_{p_np_n'}(z_n)\right\rangle \\ &\qquad - \left\langle \mathcal{G}_{il}(z_2)\mathcal{G}_{p_3p_3'}(z_3)\ldots\mathcal{G}_{p_np_n'}(z_n)\right\rangle, \end{aligned} \quad (14)$$

which link $L^{(n)}$ with $L^{(n-1)}$. All these Ward-type identities are supposed to hold if the disorder-averaging method is consistent on all levels. In Appendix C we shall rigorously prove that our Σ-derivable diagrammatic method indeed satisfies these identities and in Sec. III B we find in our ac transport simulation that it is these Ward-type identities that ensure the preservation of charge conservation after disorder average is performed in the transport calculation.

C. Coherent potential approximation

In this section, we combine the CPA theory with the Σ-derivable method presented in Sec. II A to derive our final numerical scheme for calculating $L^{(n)}$.

In the sense of dynamical mean field theory, CPA consists in assuming that the self-energy functional $\Sigma[G]$ is purely local in space and that it equals the one of the single-impurity Anderson model (SIAM): namely $\Sigma_{ii}[G] = \Sigma_{\rm SIAM}[G_{ii}]$ [46–48]. In other words, the average (medium) Green's function under CPA should satisfy the following functional equation:

$$G^{-1} = G_0^{-1} - \sum_i \Sigma_{\rm SIAM}[G_{ii}]. \quad (15)$$

To solve SIAM we start with its effective action:

$$S_i = \int d1d2\bar{\psi}_i(1)\left[i\frac{\partial}{\partial t_1}\delta(1,2) - \Delta_i(1,2)\right]\psi_i(2) - W(\tilde{n}_i), \quad (16)$$

where the auxiliary quantity Δ_i is usually termed as the hybridization function in the literature [46,47,49]. The self-energy $\Sigma_{\rm SIAM}[G_{ii}]$ can again be visualized by the diagrams shown in Fig. 1(a), but with all vertices restricted on the ith site [46,48]. The analytical expression of $\Sigma_{\rm SIAM}[G_{ii}]$ is in general very hard to approach and thus the functional relation between $\Sigma_{\rm SIAM}$ and G_{ii} can only be obtained in a numerical manner. The procedure goes as follows. By unfolding $W(\tilde{n}_i)$ using its explicit expression [see Eq. (A2)], the SIAM Green's function can be solved exactly by brute-force averaging [40,49]:

$$\begin{aligned}G^{k_1,k_{1'}}_{{\rm SIAM},i}(\omega) &= -i\int dt\ e^{i\omega t}\left\langle \psi_i^{k_1}(t)\bar{\psi}_i^{k_{1'}}(0)\right\rangle_{S_i} \\ &= \int dv_i\ p(v_i)g^{k_1,k_{1'}}_{v_i}(\omega), \end{aligned} \quad (17)$$

where k_1 and $k_{1'}$ denote Keldysh components, and g_{v_i} is a 2×2 matrix defined in the Keldysh space [20,27,28]:

$$\begin{aligned}g_{v_i}(\omega) &\equiv (\omega - V_i - \Delta_i)^{-1} \\ &= \begin{bmatrix}\omega - v_i - \Delta_i^R(\omega) & -\Delta_i^K(\omega) \\ 0 & \omega - v_i - \Delta_i^A(\omega)\end{bmatrix}^{-1}. \end{aligned} \quad (18)$$

Here all relevant quantities have been transformed into the frequency domain, since we only consider steady systems in this paper; the two-time-dependent version of the single-particle CPA theory can be formulated in parallel with Ref. [47] in a straightforward manner. Next, the SIAM self-energy is obtained from the Dyson equation [46,47]:

$$\Sigma_{{\rm SIAM},i}(\omega) = \omega - \Delta_i(\omega) - G^{-1}_{{\rm SIAM},i}(\omega). \quad (19)$$

Therefore, by specifying the value of Δ_i, both $G_{\rm SIAM}$ and its corresponding $\Sigma_{\rm SIAM}$ can be exactly calculated. In other words, the functional $\Sigma_{\rm SIAM}[G_{ii}]$ can be expressed in the form of a numerical table by sweeping the Δ_i parameter, which in this sense just plays the role of a dummy variable never entering the final form of $\Sigma_{\rm SIAM}[G_{ii}]$. Thus Eqs. (15), (17), and (19), together with the self-consistent condition $G_{{\rm SIAM},i} = G_{ii}$, form a closed set of equations, from which the solutions of Δ_i, Σ_{ii}, and G can all be obtained [27].

Now we turn to look into how to get the higher-order kernels $K^{(n)}$ in the CPA framework. As stated above, for consistency concerns, all the $K^{(n)}[G]$ should be derived from the self-energy $\Sigma[G]$:

$$K^{(n+1)}[G] = \sum_i K^{(n+1)}_{\rm SIAM}[G_{ii}] = \sum_i \frac{\delta^n \Sigma_{\rm SIAM}}{\delta G_{ii}^n}.$$

Deriving $K^{(n)}_{\rm SIAM}[G_{ii}]$ from $\Sigma_{\rm SIAM}[G_{ii}]$ analytically is rather formidable since the analytical expression of $\Sigma_{\rm SIAM}[G_{ii}]$ is generally unavailable. This problem can be circumvented by exploiting the fact that $K^{(n)}_{\rm SIAM}$ must be the *exact* kernel for the local correlator

$$L_i^{(n)} = \int dv_i\, p(v_i) g^{k_1,k_{1'}}_{v_i}(\omega_1) g^{k_2,k_{2'}}_{v_i}(\omega_2)\ldots g^{k_n,k_{n'}}_{v_i}(\omega_n), \quad (20)$$

which can be computed *exactly* by means of brute-force averaging. Therefore, given the SIAM local correlators we can solve for the corresponding kernels $K^{(n)}_{\rm SIAM}$ by running the program inversely using the same set of diagrams presented in Fig. 3. After the SIAM problem has been solved, we plug $K^{(n)}[G] = \sum_i K^{(n)}_{\rm SIAM}[G_{ii}]$ back into those diagrams (Fig. 3) and hence all the correlators $L^{(n)}$ can be calculated. The CPA numerical scheme is summarized as follows:

(1) Make an initial guess for Δ, including Δ^R and Δ^K.

(2) Calculate the local Green's function $G_{\rm SIAM}$ using Eqs. (17) and (18).

(3) Calculate $\Sigma_{\rm SIAM}$ using Eq. (19).

(4) Calculate the CPA medium Green's function G via Eq. (15).

(5) Substitute the local part of G for $G_{\rm SIAM}$ in Eq. (19) and update Δ.

(6) Go back to step 2 and iterate the procedures until Δ is fully converged.

(7) Use the converged Δ to compute $L_i^{(n)}$ via Eqs. (18) and (20).

(8) Restrict Eqs. (B1)–(B4) on single sites: For each site i substitute $L_i^{(n)}$ for $L^{(n)}$ and G_{ii} for G to solve for $K^{(n)}_{{\rm SIAM},i}$.

(9) Plug $K^{(n)}_{\rm SIAM}$ back into Eqs. (B1)–(B4) while using the full CPA medium Green's function G to obtain $L^{(n)}$.

Before closing this section, it is worth remarking on the limitation of the CPA method. Although the numerical accuracy achieved by CPA in transport calculations of various disordered nanostructures is remarkable [13,20,26–29], it is well known that due to its single-site nature CPA is unable to capture nonlocal correlation effects such as band tailing, localization, and universal fluctuation [40,50]. Admittedly, retrieving nonlocal correlations omitted by CPA on different length scales while keeping the numerical algorithm economical is a nontrivial task and still remains an open problem [40,45,49–52]. However, we would like to stress that the Σ-derivable approach presented in Sec. II A is a general diagrammatic theory. Whereas in the CPA formalism only self-energy diagrams that are spatially local (from $\Sigma_{\rm SIAM}$) are taken into account, it is possible to add nonlocal self-energies on top of $\Sigma_{\rm SIAM}$ to restore nonlocal correlations to some extent [40,50]. After the self-energy functional $\Sigma[G]$ is constructed, kernels for higher-order Green's function correlators can hence be derived according to Eq. (11).

III. APPLICATIONS

As an example, we implement our method presented above for a tight-binding chain model of a disordered two-probe transport junction as depicted in Fig. 4. The Hamiltonian for such system is partitioned as follows [3]:

$$\begin{aligned} H &= H_{\rm cen} + H_{\rm lead} + H_{\rm T},\\ H_{\rm cen} &= \sum_i v_i d_i^\dagger d_i + \sum_{\langle ij\rangle} \theta d_i^\dagger d_j,\\ H_{\rm lead} &= \sum_{\alpha\in L,R} (\varepsilon_\alpha - \mu_\alpha) c_{i\alpha}^\dagger c_{i\alpha} + \sum_{\langle ij\rangle,\alpha} \theta c_{i\alpha}^\dagger c_{j\alpha},\\ H_{\rm T} &= \sum_{\langle ij\rangle,\alpha} \theta c_{i\alpha}^\dagger d_j + {\rm H.c.}, \end{aligned}$$

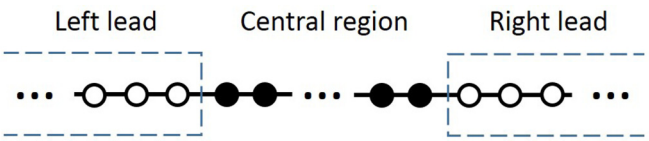

FIG. 4. Diagram of the tight-binding chain model. The external leads are disorder free while the central region contains disordered sites.

where θ is the nearest-neighbor hopping probability. The leads are assumed to be disorder free and the disorder enters the model only through the onsite term of the central region Hamiltonian. Each disorder site can be occupied either by the atomic species A or by B, with a probability $x_{A/B} = 0.5 \pm (0.5 - x)$ and an onsite energy $\varepsilon_{A/B}$.

The Hamiltonian of the leads $H_{\rm lead}$ can be folded into the central region with the standard procedure [2,27] and the resulting medium Green's functions of the central region read [5,13,27]

$$\begin{aligned} G^{R,A}(E) &= \left[E \pm i0^+ - H_{\rm cen} - \Sigma_{LR}^{R,A}(E) - \Sigma^{R,A}(E)\right]^{-1},\\ G^K(E) &= G^R(E)\left[\Sigma_{LR}^K(E) + \Sigma^K(E)\right]G^A(E), \end{aligned}$$

where $\Sigma_{LR} = \Sigma_L + \Sigma_R$ is the lead self-energy and Σ is the self-energy due to disorder. The quantum statistical information of leads is encoded in the lesser lead self-energy

$$\Sigma_{LR}^<(E) = i[f_L(E)\Gamma_L(E) + f_R(E)\Gamma_R(E)],$$

where $\Gamma_{L/R} \equiv i[\Sigma_{L/R}^R - \Sigma_{L/R}^A]$ is the linewidth function [2,3] and $f_{L/R}$ denotes the Fermi-Dirac distribution in the left/right lead. In the subsequent numerical simulations the temperature is set at 0 K and we set $\varepsilon_{L/R} = \mu_{L/R} = 0$ when the system is at equilibrium. A lesser function, generally denoted by $F^<$, is related to other components via [8]

$$F^< = \tfrac{1}{2}(-F^R + F^A + F^K). \tag{21}$$

It is worth mentioning that the transport junction model offers a platform for checking the interlevel consistency of our diagrammatic method: Due to the Keldysh relation [2,3], the identities

$$\begin{aligned} G^K &= \left\langle \mathcal{G}^R \Sigma_{LR}^K \mathcal{G}^A \right\rangle_{L^{(2)}},\\ \langle \mathcal{G}^K \mathcal{G}^{R,A}\rangle_{L^{(2)}} &= \left\langle \mathcal{G}^R \Sigma_{LR}^K \mathcal{G}^A \mathcal{G}^{R,A}\right\rangle_{L^{(3)}},\\ \langle \mathcal{G}^K \mathcal{G}^K\rangle_{L^{(2)}} &= \left\langle \mathcal{G}^R \Sigma_{LR}^K \mathcal{G}^A \mathcal{G}^R \Sigma_{LR}^K \mathcal{G}^A\right\rangle_{L^{(4)}}, \end{aligned} \tag{22}$$

where $\mathcal{G}$ denotes the Green's function of the central region under a specified atomic configuration, must hold if the consistency is respected; these identities have been checked to very high precision in our numerical simulations.

A. Moments of the transmission probability distribution

As can be deduced from the Landauer-Büttiker formula [2]

$$I = \int \frac{dE}{2\pi} T(E)[f_L(E) - f_R(E)],$$

the dc conductance of the system under low bias is determined by the transmission coefficient [2]

$$T(E) \equiv {\rm Tr}[\mathcal{G}^R \Gamma_L \mathcal{G}^A \Gamma_R]. \tag{23}$$

Therefore, the first step toward portraying the probability distribution of the dc conductance in the presence of random disorder is to calculate the moments $\langle T^n(E)\rangle$. Equation (23) can be converted into a more compact form, $T(E) = {\rm Tr}[\mathcal{G}^< \Gamma_R]$, if one assumes $f_L(E) = 1$ and $f_R(E) = 0$ during the numerical procedure [20,27]. In this way, the moments can be expressed as

$$\langle T^n\rangle = \langle [{\rm Tr}(\mathcal{G}^< \Gamma_R)]^n\rangle. \tag{24}$$

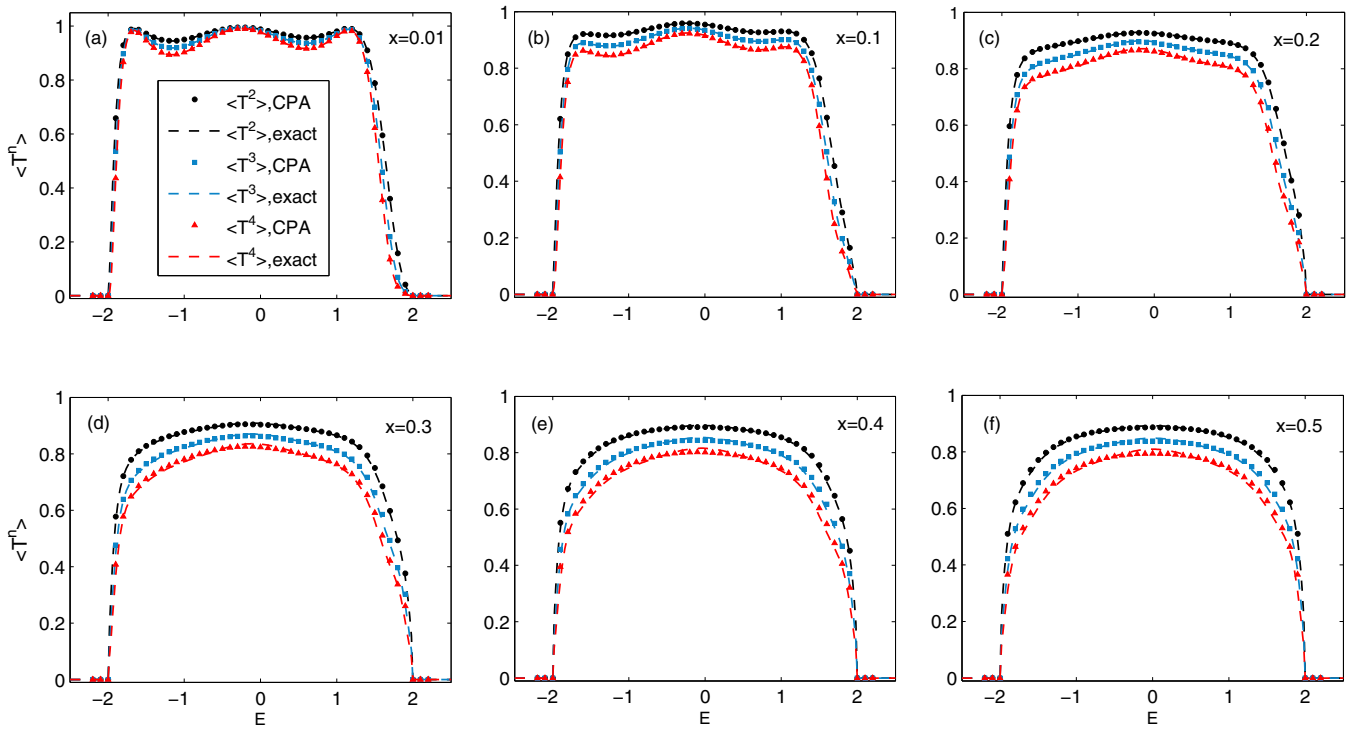

FIG. 5. Disorder-induced transmission moments $\langle T^n(E)\rangle$ of a tight-binding transport junction containing four disordered sites in its central region. The numerical results are obtained with two methods: CPA and brute-force computation. The onsite energies of the two atomic species are $\varepsilon_{A/B} = \mp 0.25\theta$ and the disorder concentration x varies from 0.01 to 0.5. The energy (E) is in units of the hopping probability (θ).

With the aid of Eq. (21), it can be immediately seen that Eq. (24) can be computed by means of $L^{(n)}$.

Using both our CPA-based theoretical scheme presented in the last section and the brute-force computation, we evaluated up to $\langle T^4(E)\rangle$ for a one-dimensional transport junction with four disordered sites in the central region. The on-site energies are $\varepsilon_{A/B} = \mp 0.25\theta$ [53,54] and the concentration x varies from 0.01 to 0.5. Numerical results are shown in Fig. 5. In the brute-force computation, all possible disorder configurations are calculated to obtain the exact average results. By comparing to the exact results, it can be seen in the plot that our CPA-based method works very well at all impurity concentrations. As the calculations involve all types of correlators up to $L^{(4)}$, the accuracy of our CPA-based method is therefore verified. Furthermore, we find that our CPA results satisfy the basic inequality $\langle T^n(E)\rangle - \langle T(E)\rangle^n \geqslant 0$, which could be violated at relatively high impurity concentrations by the SSA-based method as known before [5]. From Fig. 5, at high impurity concentrations ($x \geqslant 0.3$), curves of the exact results (e.g., $\langle T^3(E)\rangle$ and $\langle T^4(E)\rangle$) around $E = 0$ exhibit a very slight lump shape, which our CPA-based method does not capture. This tiny difference may be attributed to nonlocal interference effects of the impurity scattering which is beyond the local mean-field theory presented here [18,40,45,49]. Nevertheless, the Σ-derivable theory presented in this paper serves as a universal guidance on how to construct diagrams consistently.

B. Disorder-averaged ac conductance

The dynamic ac conductance $D^c_{\alpha\beta}$ is defined via the linear response relation $I^c_\alpha(\Omega) = \sum_\beta D^c_{\alpha\beta}(\Omega)v_\beta(\Omega)$, where Ω is the response frequency, I^c_α denotes the charge current in lead α, and v_α denotes the applied voltage. By Green's function theory, the dynamic ac conductance can be expressed as [55–57]

$$\begin{aligned} D^c_{\alpha\beta}(\Omega,E) = -\int \frac{dE}{2\pi}\mathrm{Tr}\big[&\mathbb{G}^<_\beta\big(\Sigma^A_\alpha - \Sigma^R_{\alpha+}\big) + \mathbb{G}^R_\beta\Sigma^<_\alpha \\ &- \mathbb{G}^A_\beta\Sigma^<_{\alpha+} + \delta_{\alpha\beta}\big(\mathcal{G}^R_+\sigma^<_\alpha - \mathcal{G}^A\sigma^<_\alpha \\ &+ \mathcal{G}^<_+\sigma^A_\alpha - \mathcal{G}^<\sigma^R_\alpha\big)\big], \end{aligned} \tag{25}$$

where the abbreviation $\Sigma^\gamma_{\alpha+}$ denotes $\Sigma^\gamma_\alpha(E+\Omega)$ ($\gamma = R/A/<$), and similarly $\mathcal{G}^\gamma_+ \equiv \mathcal{G}^\gamma(E+\Omega)$. $\mathbb{G}^\gamma_\beta(E)$ is defined as

$$\begin{aligned} \mathbb{G}^{R,A}_\beta(E) &= \mathcal{G}^{R,A}(E+\Omega)\sigma^{R,A}_\beta(E)\mathcal{G}^{R,A}(E), \\ \mathbb{G}^<_\beta(E) &= \mathcal{G}^R(E+\Omega)\sigma^<_\beta(E)\mathcal{G}^A(E) \\ &\quad + \mathcal{G}^R(E+\Omega)\sigma^R_\beta(E)\mathcal{G}^<(E) \\ &\quad + \mathcal{G}^<(E+\Omega)\sigma^A_\beta(E)\mathcal{G}^A(E) \\ \sigma^\gamma_\beta(E) &= \big[\Sigma^\gamma_\beta(E) - \Sigma^\gamma_\beta(E+\Omega)\big]/\Omega. \end{aligned}$$

As Eq. (25) involves products of various real-time Green's functions, it is necessary to employ the disorder-averaging method derived in Sec. II for the evaluation of the average conductance $\langle D^c_{\alpha\beta}\rangle$. Note that for correlators $\langle\mathcal{G}^<(E+\Omega)\mathcal{G}^A(E)\rangle$ and $\langle\mathcal{G}^R(E+\Omega)\mathcal{G}^<(E)\rangle$, which are involved via $\mathbb{G}^<_\beta(E)$, either $L^{(2)}$ or $L^{(3)}$ can be used; the applicability of $L^{(3)}$ in this context is due to the fact that $\mathcal{G}^<$ can be expanded as $\mathcal{G}^< = \mathcal{G}^R\Sigma^<_{LR}\mathcal{G}^A$ [2,3]. We have checked to high numerical precision that both methods yield exactly the same result, as required by the

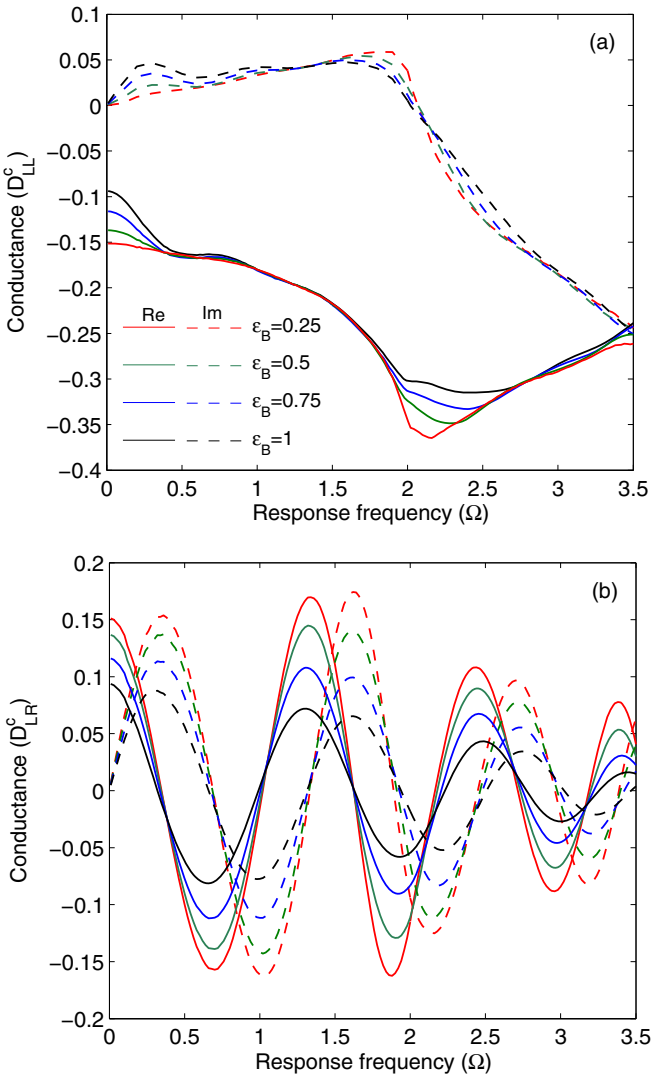

FIG. 6. Disorder-averaged ac dynamic conductance (vs response frequency Ω) of a one-dimensional transport junction with nine disordered sites in the central region. Each disordered site can be occupied either by species A or species B with an equal probability and the onsite energy of A is fixed at the equilibrium chemical potential, i.e., $\varepsilon_A = 0$, while ε_B is adjustable. The solid (dashed) lines denote the real (imaginary) part of the conductance. The response frequency (Ω) is in unit of $\theta/\hbar$, where θ is the hopping probability.

interlevel diagrammatic consistency. It should be pointed out that $L^{(2)}$ is easier for numerical implementation while $L^{(3)}$ is useful for elucidating the conservation consistency of the theory (to be explained later).

As a concrete example, we consider the one-dimensional transport junction with nine disordered sites in the central region, where each disordered site can be occupied by species A or B with an equal probability ($x = 0.5$). The onsite energy of species A is fixed at the Fermi energy ($\varepsilon_A = 0$) while ε_B is adjustable: The disorder scattering can be intensified by increasing ε_B. Both the real and imaginary parts of the CPA-averaged $D^c_{LL/LR}$ are plotted in Fig. 6 as a function of Ω.

We first look at the dc limit, i.e., $\Omega \to 0$, where we observe that both $\mathrm{Im}\langle D^c_{LL}\rangle$ and $\mathrm{Im}\langle D^c_{LR}\rangle$ approach to zero no matter how strong the disorder scattering is, which confirms the fact that in dc limit the transport junction displays a pure resistance-like property. Another observation at $\Omega \to 0$ is that the real parts $\mathrm{Re}\langle D^c_{LL}\rangle$ and $\mathrm{Re}\langle D^c_{LR}\rangle$ both coincide with the disorder-averaged dc transmission coefficient.

Interestingly, for $\mathrm{Re}\langle D^c_{LL}\rangle$ [Fig. 6(a)] we find a frequency range $\Omega \in [0.5, 1.8] \cup [2.7, 3.25]$ where the value of $\mathrm{Re}\langle D^c_{LL}\rangle$ has a very weak dependence on the disorder strength, indicating that for the given electron energy, the related high-frequency transport is governed by a response length scale that is shorter than the disorder limited mean-free-path. In Fig. 6(b) a typical oscillation profile of both $\mathrm{Re}\langle D^c_{LR}\rangle$ and $\mathrm{Im}\langle D^c_{LR}\rangle$ as functions of Ω is observed. Similar oscillating profiles have been reported before for a variety of ac transport junctions with a finite central device region [58–63]. This phenomenon is usually attributed to the photon-assisted tunneling effect [56,63,64]. As can be seen in Fig. 6(b), introducing disorder does not destroy the oscillation profile, although both the amplitude and the position of the tunneling peaks are altered due to the disorder strength. This simply reflects the fact that disorder scattering influences both the width and the position of quasiparticle energy levels in the central device region [29].

Before closing this section, we provide another consistency check of our theory from the perspective of charge conservation. In the linear response ac transport theory, charge conservation requires that [55,56]

$$\sum\nolimits_\alpha D^c_{\alpha\beta} = \Omega \int \frac{dE}{2\pi} \mathrm{Tr}[\mathbb{G}^<_\beta]. \tag{26}$$

Namely, the charge accumulation rate in the central device region should equal to the net incident current. Upon taking disorder average on both sides, Eq. (26) is supposed to be preserved if conservation consistency is respected by the disorder-averaging method, as Eq. (26) involves Green's function correlators of different types. We have numerically checked that our CPA-based method does meet this requirement and, analytically, it can be verified as follows. By writing $\mathcal{G}^<$ as $\mathcal{G}^R \Sigma^<_{LR} \mathcal{G}^A$ and then employing the cyclical property of the trace operator, the conservation requirement Eq. (26) is equated with

$$\begin{aligned} 0 = {} & \sigma^<_\beta \langle \mathcal{G}^A \big(\Sigma^A_{LR} - \Sigma^R_{LR+} + \Omega\big) \mathcal{G}^R_+ \rangle \\ & + \sigma^R_\beta \langle \mathcal{G}^R \Sigma^<_{LR} \mathcal{G}^A \big(\Sigma^A_{LR} - \Sigma^R_{LR+} + \Omega\big) \mathcal{G}^R_+ \rangle \\ & + \sigma^A_\beta \langle \mathcal{G}^A \big(\Sigma^A_{LR} - \Sigma^R_{LR+} + \Omega\big) \mathcal{G}^R_+ \Sigma^R_{LR+} \mathcal{G}^A_+ \rangle \\ & + \sigma^R_\beta \langle \mathcal{G}^R \Sigma^<_{LR} \mathcal{G}^R_+ \rangle - \sigma^A_\beta \langle \mathcal{G}^A \Sigma^<_{LR+} \mathcal{G}^A_+ \rangle \\ & + \sigma^<_\beta G^R_+ - \sigma^<_\beta G^A + \sigma^A_\beta G^<_+ - \sigma^R_\beta G^<. \end{aligned} \tag{27}$$

By means of substitution

$$\begin{aligned} \Sigma^A_{LR} - \Sigma^R_{LR+} + \Omega &= \big[G^R_0(E+\Omega)\big]^{-1} - \big[G^A_0(E)\big]^{-1} \\ &= C(E - i0^+, E + i0^+ + \Omega), \end{aligned}$$

Eq. (27) can be easily verified by employing the Ward identities (C1) and (C8) presented in the appendix. Therefore, the charge conservation of ac transport in disordered systems is confirmed under our formalism.

IV. SUMMARY

Solving the problem of multiple impurity effects in quantum transport of atomic nanostructures is a very important but difficult theoretical challenge. To this end significant progress has been achieved in recent years where CPA has been combined with atomic first principles methods to make material specific predictions of disorder effects in quantum transport of nanoelectronic devices. So far, existing two-particle CPA theories have relied on the single-site decoupling approximation (SSA) [11,13,20], which may bring consistency and accuracy issues when extended for calculating the disorder-average of higher order Green's function correlators. In addition, existing theories beyond two-particle CPA have not dealt with correlators containing the Keldysh component of the Green's function, which appears in many theoretical derivations of quantum transport formulas. This work advances a theoretical formulation that solves these theoretical problems lying in the current CPA formalism.

In particular, here we report a Feynman diagrammatic approach for calculating the configurationally averaged Green's function correlators that widely appear in quantum transport theories of disordered nanostructures. Our theory treats equilibrium and nonequilibrium quantum statistics on an equal footing by taking into account the Keldysh Green's function in a unified manner. The theory emphasizes on two consistency requirements. The first is an interlevel consistency for diagrams at different levels of the correlators: Namely if a physical quantity can be evaluated in two ways using diagrams belonging to different $L^{(n)}$, we demand that the final results agree precisely. The second regards the conservation consistency of transport calculations, which amounts to requiring that the disorder-averaged charge continuity equation be satisfied. These are found to be bonded with the satisfaction of a set of Ward-like identities, which are very strong demands to be imposed on a diagrammatic theory.

This theory is then applied to a tight binding atomic model with disorder to calculate its quantum transport properties such as ac conductance and higher order moments of the transmission probability distribution. The results agree at very high precision with the exact results obtained from enumerating all possible disorder configurations. Therefore, we conclude that our formalism can be applied to predict both dc and ac quantum transport properties of disorder-containing nanoelectronic devices.

ACKNOWLEDGMENTS

We thank Dr. Youqi Ke for useful discussions on Ref. [20] and CPA theory. We gratefully acknowledge financial support by the Natural Sciences and Engineering Research Council of Canada (H.G.). We thank CalcuQuebec and Compute Canada for computation facilities.

APPENDIX A: BASICS OF THE KELDYSH PATH-INTEGRAL METHOD FOR THE DISORDER-AVERAGING PROBLEM

The timeline used in the Keldysh formalism is the so-called closed time contour [9] as depicted in Fig. 7. A time dependence is assigned to the Hamiltonian defined along the contour

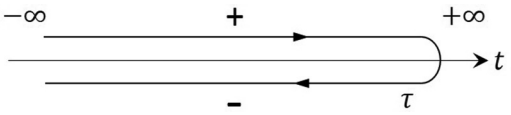

FIG. 7. Diagram of the closed time contour used in the Keldysh formalism. The contour begins and ends both at $-\infty$. It consists of a forward branch (denoted by $+$) and a backward branch (denoted by $-$). The complex time is denoted by τ as opposed to t for the real time.

$$H(\tau) = H_0(\tau) + \sum\nolimits_i v_i(\tau) a_i^\dagger a_i,$$

where τ is a complex-time variable and $H_0(\tau)$ is the Hamiltonian of the clean system. $v_i(\tau)$ denotes the quenched impurity potential which is assumed to be switched on and off adiabatically: $v_i(\tau) = e^{-\eta|\tau|} v_i$, where η is an infinitesimal positive number [9]. Note that $H(\tau)$ is the same at τ^+ and τ^-. At $\tau \to -\infty$ the system is assumed to be at equilibrium with the density matrix $\rho_0 = e^{-\beta H_0(-\infty)}/Z_0$, where the partition function $Z_0 \equiv \mathrm{Tr}\{e^{-\beta H_0(-\infty)}\}$.

In the path-integral language, the n-particle Green's function under a given impurity potential is expressed as [9,37,38]

$$\begin{aligned} &\mathcal{G}_v^{(n)}(1,\ldots,n;1',\ldots,n') \\ &\quad \equiv \frac{1}{i^n}\langle \psi(1)\ldots\psi(n)\bar{\psi}(n')\ldots\bar{\psi}(1')\rangle_v \\ &\quad = \frac{1}{i^n} Z_0^{-1} \int D[\psi,\bar{\psi}] e^{iS_0 - iS_v} \psi(1)\ldots\psi(n) \\ &\qquad \times \bar{\psi}(n')\ldots\bar{\psi}(1'), \end{aligned} \tag{A1}$$

where $1,\ldots,n$ are space-time collective indices of the form (i,τ), and ψ and $\bar{\psi}$ are respectively the Grassmann variable assigned to the collective index and its conjugate. The actions in Eq. (A1) are defined as [9,38]

$$S_0 = \int_C d\tau_1' d\tau_2' \sum_{ij} \bar{\psi}_i(\tau_1') G_{0,ij}^{-1}(\tau_1',\tau_2') \psi_j(\tau_2')$$

$$S_v = \int_C d\tau' \sum_i v_i(\tau') \bar{\psi}_i(\tau') \psi_i(\tau'),$$

where G_0 is the contour-ordered single-particle Green's function [9] of the clean system which satisfies the equation of motion

$$i\partial_{\tau_1} G_{0,ij}(\tau_1,\tau_2) - \sum\nolimits_k H_{0,ik}(\tau_1) G_{0,kj}(\tau_1,\tau_2) = \delta_{ij}\delta(\tau_1-\tau_2).$$

on the contour [3].

One major advantage of using the Keldysh technique for the disorder-averaging problem is that the normalization factor in Eq. (A1), namely Z_0, is disorder independent due to the adiabatic assumption [9], while in the imaginary-time formalism one has to resort to the replica trick in order to deal with the disorder-dependent normalization factor therein [39]. Thus the disorder-average of (A1) is achieved by simply

replacing S_v with [40,49]

$$\begin{aligned} S_{\rm d} &= \sum\nolimits_i W(\tilde{n}_i), \\ W(\tilde{n}_i) &\equiv -\ln \int dv_i \;\; p(v_i)\exp(-v_i\tilde{n}_i) \\ &= \sum_{l=2}^{\infty} \frac{1}{l!}\langle v_i^l\rangle_c (\tilde{n}_i)^l, \end{aligned} \tag{A2}$$

where $\langle v_i^l\rangle_c$ is the lth cumulant of the impurity potential probability distribution $p(v_i)$ and

$$\tilde{n}_i \equiv \int_C d\tau' \bar{\psi}_i(\tau')\psi_i(\tau').$$

For convenience of diagram constructions of Green's functions, we shall explore the expression of the normalization factor Z_0 in the path-integral language. Taking $n = 0$ in Eq. (A1) one sees $Z_0 = \int D[\psi,\bar{\psi}]e^{iS_0 - iS_v}$. Note that this does not mean Z_0 is dependent of the impurity potential: in fact the S_v part makes no contribution because its integral on the backward branch of the contour exactly cancels the one on the forward branch [9,37]. As such, one can further write down $Z_0 = \int D[\psi,\bar{\psi}]e^{iS_0 - iS_{\rm d}}$ upon taking disorder-average. Thus the disorder-averaged n-particle Green's function defined on the closed time contour can be expressed as

$$\begin{aligned} &G^{(n)}(1,\ldots,n;1',\ldots,n') \\ &= \frac{1}{i^n}\frac{\int D[\psi,\bar{\psi}]e^{i(S_0-S_{\rm d})}\psi(1)\ldots\psi(n)\bar{\psi}(n')\ldots\bar{\psi}(1')}{\int D[\psi,\bar{\psi}]e^{i(S_0-S_{\rm d})}}. \end{aligned} \tag{A3}$$

In practice one also defines real-time (single-particle) Green's functions as follows: $G^{<}_{ij}(t,t') \equiv -i\langle\psi_i^+(t)\bar{\psi}_j^-(t')\rangle$, $G^{>}_{ij}(t,t') \equiv -i\langle\psi_i^-(t)\bar{\psi}_j^+(t')\rangle$, $G^{\mathbb{T}}_{ij}(t,t') \equiv -i\langle\psi_i^+(t)\bar{\psi}_j^+(t')\rangle$, and $G^{\bar{\mathbb{T}}}_{ij}(t,t') \equiv -i\langle\psi_i^-(t)\bar{\psi}_j^-(t')\rangle$. The contour-ordered single-particle Green's function can then be expressed in a matrix form: $G = \left(\begin{smallmatrix} G^{\mathbb{T}} & G^{<} \\ G^{>} & G^{\bar{\mathbb{T}}}\end{smallmatrix}\right)$ [9,28].

For the diagrammatic construction of the disorder-averaging problem, it is often more favorable to use another set of Grassmann variables: $\psi^{\rm cl}(t) = [\psi^+(t) + \psi^-(t)]/\sqrt{2}$, $\psi^{\rm q}(t) = [\psi^+(t) - \psi^-(t)]/\sqrt{2}$, $\bar{\psi}^{\rm cl}(t) = [\bar{\psi}^+(t) - \bar{\psi}^-(t)]/\sqrt{2}$, and $\bar{\psi}^{\rm q}(t) = [\bar{\psi}^+(t) + \bar{\psi}^-(t)]/\sqrt{2}$, where the superscripts "cl" stands for classical and "q" for quantum [9]. This linear transformation is termed as the Keldysh rotation in the literature [9]. A new set of real-time Green's functions are hence introduced [9]:

$$\begin{aligned} G_{ij}^{\rm cl,cl(R)}(t,t') &= -i\left\langle\psi_i^{\rm cl}(t)\bar{\psi}_j^{\rm cl}(t')\right\rangle, \\ G_{ij}^{\rm q,q(A)}(t,t') &= -i\left\langle\psi_i^{\rm q}(t)\bar{\psi}_j^{\rm q}(t')\right\rangle, \\ G_{ij}^{\rm cl,q(K)}(t,t') &= -i\left\langle\psi_i^{\rm cl}(t)\bar{\psi}_j^{\rm q}(t')\right\rangle. \end{aligned} \tag{A4}$$

After Keldysh rotation, the matrix single-particle Green's function is transformed into a triangular form: $G = \left(\begin{smallmatrix} G^R & G^K \\ 0 & G^A\end{smallmatrix}\right)$ [9,28]. The expression of the n-particle Green's function remains formally unchanged as of Eq. (A3). However, now each collective index acquires a field component that takes either cl or q, and the complex-time variable is replaced with the real-time variable. Besides, S_0 should be transformed into [9]

$$S_0 = \int_{-\infty}^{+\infty} dt_1' dt_2' \sum_{k_1,k_2}\sum_{ij} \bar{\psi}_i^{k_1}(t_1')\left(G_0^{-1}\right)_{ij}^{k_1k_2}(t_1',t_2')\psi_j^{k_2}(t_2'), \tag{A5}$$

where k_1 and k_2 denote cl or q, and $\tilde{n}_i$ is re-expressed as

$$\tilde{n}_i = \int_{-\infty}^{+\infty} dt'\left[\bar{\psi}_i^{\rm cl}(t')\psi_i^{\rm cl}(t') + \bar{\psi}_i^{\rm q}(t')\psi_i^{\rm q}(t')\right] \tag{A6}$$

in terms of the cl/q-field components.

APPENDIX B: EXPRESSIONS OF $L^{(2)}$, $L^{(3)}$, AND $L^{(4)}$

Equations in this Appendix are formulated in accordance with the diagrams presented in Fig. 3. In what follows, repeated indices (denoted by overlines) are assumed to be integrated over:

$$\begin{aligned} L^{(2)}(11'22') &= G(11')G(22') \\ &\quad + G(1\bar{3})G(\bar{4}2')K^{(2)}(\bar{3}\bar{6}\bar{5}\bar{4})L^{(2)}(\bar{6}1'2\bar{5}), \end{aligned} \tag{B1}$$

$$\begin{aligned} A^{(2)}(11'22') &= \delta(11')\delta(22') + K^{(2)}(1\bar{1}\bar{2}2')L^{(2)}(\bar{1}1'2\bar{2}), \\ A^{(3)}(11',22',33') &= A^{(2)}(\bar{3}'3'11')G(\bar{3}\bar{3}')A^{(2)}(22'3\bar{3}) \\ &\quad + L^{(2)}(\bar{3}'3'1\bar{1})K^{(3)}(\bar{1}1',2\bar{2}',\bar{3}\bar{3}') \\ &\quad \times L^{(2)}(\bar{2}'2'3\bar{3}), \end{aligned} \tag{B2}$$

$$L^{(3)}(11',22',33') = A^{(3)}(1\bar{1},\bar{2}2',33')L^{(2)}(\bar{1}1'2\bar{2}), \tag{B3}$$

$$\begin{aligned} &L^{(4)}(11',22',33',44') \\ &= A^{(3)}(2\bar{2},\bar{4}'4',11')L^{(2)}(\bar{2}\bar{2}'\bar{4}\bar{4}')A^{(3)}(4\bar{4},\bar{2}'2',33') \\ &\quad + A^{(3)}(3\bar{3},\bar{1}'1',22')L^{(2)}(\bar{1}\bar{1}'\bar{3}\bar{3}')A^{(3)}(1\bar{1},\bar{3}'3',44') \\ &\quad - G(\bar{4}\bar{4}')A^{(2)}(\bar{4}'4'1\bar{1})G(\bar{1}\bar{1}')A^{(2)}(\bar{1}'1'2\bar{2})G(\bar{2}\bar{2}') \\ &\quad \times A^{(2)}(\bar{2}'2'3\bar{3})G(\bar{3}\bar{3}')A^{(2)}(\bar{3}'3'4\bar{4}) \\ &\quad + K^{(4)}(\bar{1}\bar{1}',\bar{2}\bar{2}',\bar{3}\bar{3}',\bar{4}\bar{4}')L^{(2)}(\bar{4}'4'1\bar{1})L^{(2)}(\bar{1}'1'2\bar{2}) \\ &\quad \times L^{(2)}(\bar{2}'2'3\bar{3})L^{(2)}(\bar{3}'3'4\bar{4}). \end{aligned} \tag{B4}$$

APPENDIX C: PROOF OF WARD-TYPE IDENTITIES

We start with the Ward-identity of lowest order:

$$\begin{aligned} G_{il}(z_1) - G_{il}(z_2) &= \langle\mathcal{G}_{ij}(z_1)C_{jk}(z_1,z_2)\mathcal{G}_{kl}(z_2)\rangle \\ &\quad \left[\equiv L^{(2)}_{ijkl}(z_1,z_2)C_{jk}(z_1,z_2)\right], \end{aligned} \tag{C1}$$

where $C(z_1,z_2) \equiv [G_0(z_2)]^{-1} - [G_0(z_1)]^{-1}$. To prove Eq. (C1), we first notice from Eq. (7) that the right-hand side of Eq. (C1) can be rewritten as [11]

$$\begin{aligned} &L^{(2)}_{ijkl}(z_1,z_2)C_{jk}(z_1,z_2) \\ &\quad = G_{ij}(z_1)[C_{jk}(z_1,z_2) + \Lambda_{jk}(z_1,z_2)]G_{kl}(z_2), \end{aligned} \tag{C2}$$

where the vertex correction Λ satisfies the following recursive relation [37]:

$$\Lambda_{jk}(z_1,z_2) = K^{(2)}_{jlmk}(z_1,z_2)G_{lu}(z_1)[C_{uv}(z_1,z_2) + \Lambda_{uv}(z_1,z_2)]G_{vm}(z_2). \tag{C3}$$

To solve for Λ we shall utilize Vollhardt-Wölfle's theorem [43]:

$$\Sigma_{jk}(z_1) - \Sigma_{jk}(z_2) = K^{(2)}_{jlmk}(z_1,z_2)[G_{lm}(z_1) - G_{lm}(z_2)], \tag{C4}$$

which has proven valid for any Σ-derivable kernel $K^{(2)}$. The right-hand side of Eq. (C4) can be rewritten as

$$K^{(2)}_{jlmk}(z_1,z_2)G_{lu}(z_1)\big[G^{-1}_{uv}(z_2) - G^{-1}_{uv}(z_1)\big]G_{vm}(z_2).$$

Next, the quantity $[G^{-1}_{uv}(z_2) - G^{-1}_{uv}(z_1)]$ is replaced with

$$G^{-1}_{uv}(z_2) - G^{-1}_{uv}(z_1) = C_{uv}(z_1,z_2) + \Sigma_{uv}(z_1) - \Sigma_{uv}(z_2), \tag{C5}$$

where we have used the Dyson equation (15). We then arrive at

$$\Sigma_{jk}(z_1) - \Sigma_{jk}(z_2) = K^{(2)}_{jlmk}(z_1,z_2)G_{lu}(z_1)[C_{uv}(z_1,z_2) + \Sigma_{uv}(z_1) - \Sigma_{uv}(z_2)]G_{vm}(z_2). \tag{C6}$$

It can be immediately seen that Eq. (C6) is of the same form as the recursive relation Eq. (C3) with $\Lambda(z_1,z_2)$ replaced with $[\Sigma(z_1) - \Sigma(z_2)]$. Since Eq. (C3) is an inhomogeneous linear equation for Λ, its solution is uniquely determined [5,29]:

$$\Lambda_{jk}(z_1,z_2) = \Sigma_{jk}(z_1) - \Sigma_{jk}(z_2). \tag{C7}$$

Inserting Eq. (C7) into Eq. (C2) and utilizing Eq. (C5) again, we arrive at Eq. (C1).

Moving forward, the Ward-type identity which associates $L^{(2)}$ with $L^{(3)}$ reads

$$\langle \mathcal{G}_{il}(z_1)\mathcal{G}_{mn}(z_3)\rangle - \langle \mathcal{G}_{il}(z_2)\mathcal{G}_{mn}(z_3)\rangle = \langle \mathcal{G}_{ij}(z_1)C_{jk}(z_1,z_2)\mathcal{G}_{kl}(z_2)\mathcal{G}_{mn}(z_3)\rangle \big[\equiv L^{(3)}_{ij,kl,mn}(z_1,z_2,z_3)C_{jk}(z_1,z_2)\big]. \tag{C8}$$

To prove Eq. (C8) we start with its left-hand side. Using Eq. (8) we obtain

$$\begin{aligned}
\langle \mathcal{G}_{il}(z_1)\mathcal{G}_{mn}(z_3)\rangle - \langle \mathcal{G}_{il}(z_2)\mathcal{G}_{mn}(z_3)\rangle &= L^{(2)}_{ilmn}(z_1,z_3) - L^{(2)}_{ilmn}(z_2,z_3) \\
&= \left[\begin{pmatrix}\overrightarrow{G}(z_1)\\ \bullet\\ \overleftarrow{G}(z_3)\end{pmatrix} + \begin{pmatrix}\overrightarrow{G}(z_1)\\ \bullet\\ \overleftarrow{G}(z_3)\end{pmatrix} \odot K^{(2)}(z_1,z_3) \odot \begin{pmatrix}\overrightarrow{G}(z_1)\\ \bullet\\ \overleftarrow{G}(z_3)\end{pmatrix} + \cdots\right] \\
&\quad - \left[\begin{pmatrix}\overrightarrow{G}(z_2)\\ \bullet\\ \overleftarrow{G}(z_3)\end{pmatrix} + \begin{pmatrix}\overrightarrow{G}(z_2)\\ \bullet\\ \overleftarrow{G}(z_3)\end{pmatrix} \odot K^{(2)}(z_2,z_3) \odot \begin{pmatrix}\overrightarrow{G}(z_2)\\ \bullet\\ \overleftarrow{G}(z_3)\end{pmatrix} + \cdots\right] \\
&= \begin{pmatrix}\Delta\overrightarrow{G}\\ \bullet\\ \overleftarrow{G}(z_3)\end{pmatrix} + \begin{pmatrix}\Delta\overrightarrow{G}\\ \bullet\\ \overleftarrow{G}(z_3)\end{pmatrix} \odot K^{(2)}(z_2,z_3) \odot \begin{pmatrix}\overrightarrow{G}(z_2)\\ \bullet\\ \overleftarrow{G}(z_3)\end{pmatrix} \\
&\quad + \begin{pmatrix}\overrightarrow{G}(z_1)\\ \bullet\\ \overleftarrow{G}(z_3)\end{pmatrix} \odot [K^{(2)}(z_1,z_3) - K^{(2)}(z_2,z_3)] \odot \begin{pmatrix}\overrightarrow{G}(z_2)\\ \bullet\\ \overleftarrow{G}(z_3)\end{pmatrix} \\
&\quad + \begin{pmatrix}\overrightarrow{G}(z_1)\\ \bullet\\ \overleftarrow{G}(z_3)\end{pmatrix} \odot K^{(2)}(z_1,z_3) \odot \begin{pmatrix}\Delta\overrightarrow{G}\\ \bullet\\ \overleftarrow{G}(z_3)\end{pmatrix} + \cdots,
\end{aligned} \tag{C9}$$

where $\Delta\overrightarrow{G} \equiv \overrightarrow{G}(z_1) - \overrightarrow{G}(z_2)$ and we have employed the mathematical identity

$$\begin{aligned}
&X_1X_2\cdots X_n - Y_1Y_2\cdots Y_n \\
&\quad = X_1X_2\cdots X_{n-1}\Delta X_n + X_1X_2\cdots\Delta X_{n-1}Y_n + \cdots \\
&\qquad + \Delta X_1Y_2\cdots Y_n,
\end{aligned} \tag{C10}$$

where $\Delta X_i \equiv X_i - Y_i$. To proceed we shall look into the quantity $[K^{(2)}(z_1,z_3) - K^{(2)}(z_2,z_3)]$. Suppose $\mathcal{K}^{(2)}$ is one of the $K^{(2)}$ diagrams that contain m right-going Green's function lines (carrying energy z_1) and n left-going Green's function lines (carrying energy z_3). Then, without loss of generality, $\mathcal{K}^{(2)}$ can be formally expressed as

$$\mathcal{K}^{(2)}_{iluv}(z_1,z_3) = \overrightarrow{G}_{ip'_1}(z_1)\overrightarrow{G}_{p_2p'_2}(z_1)\cdots\overrightarrow{G}_{p_ml}(z_1) \times \overleftarrow{G}_{uq'_1}(z_3)\overleftarrow{G}_{q_2q'_2}(z_3)\cdots\overleftarrow{G}_{q_nv}(z_3)V^{\mathcal{K}},$$

where $V^{\mathcal{K}}$ is the contribution from the vertices in the diagram and is independent of the energy arguments [39,43]. By utilizing Eq. (C10) again we get

$$\begin{aligned}
&\mathcal{K}^{(2)}_{iluv}(z_1,z_3) - \mathcal{K}^{(2)}_{iluv}(z_2,z_3) \\
&\quad = \big[\overrightarrow{G}_{ip'_1}(z_1)\overrightarrow{G}_{p_2p'_2}(z_1)\cdots\Delta\overrightarrow{G}_{p_ml} + \cdots \\
&\qquad + \overrightarrow{G}_{ip'_1}(z_1)\Delta\overrightarrow{G}_{p_2p'_2}\cdots\overrightarrow{G}_{p_ml}(z_2)
\end{aligned}$$

$$+\Delta\overrightarrow{G}_{ip_1'}\overrightarrow{G}_{p_2p_2'}(z_2)\cdots\overrightarrow{G}_{p_ml}(z_2)\big]$$
$$\times\overleftarrow{G}_{uq_1'}(z_3)\overleftarrow{G}_{q_2q_2'}(z_3)\cdots\overleftarrow{G}_{q_nv}(z_3)V^{\mathcal{K}}$$
$$=\mathcal{K}^{(3)}_{ij,kl,uv}(z_1,z_2,z_3)\Delta\overrightarrow{G}_{jk}, \tag{C11}$$

where $\mathcal{K}^{(3)}$ is the collection of those $K^{(3)}$ diagrams that can be generated by removing one $\overrightarrow{G}$ line from $\mathcal{K}^{(2)}$, namely $\mathcal{K}^{(3)}=\delta\mathcal{K}^{(2)}/\delta\overrightarrow{G}$. We thus obtain the following identity with close resemblance to Eq. (C4):

$$K^{(2)}_{iluv}(z_1,z_3)-K^{(2)}_{iluv}(z_2,z_3)$$
$$=K^{(3)}_{ij,kl,uv}(z_1,z_2,z_3)[G_{jk}(z_1)-G_{jk}(z_2)], \tag{C12}$$

which should be regarded as a direct consequence of the Σ drivability imposed on $K^{(2)}$ and $K^{(3)}$. By means of Eq. (C12), Eq. (C9) reduces to

$$\langle\mathcal{G}_{il}(z_1)\mathcal{G}_{mn}(z_3)\rangle-\langle\mathcal{G}_{il}(z_2)\mathcal{G}_{mn}(z_3)\rangle$$
$$=A^{(2)}(z_1,z_3)\odot\begin{pmatrix}\Delta\overrightarrow{G}\\ \bullet\\ \overleftarrow{G}(z_3)\end{pmatrix}\odot A^{(2)}(z_2,z_3)$$
$$+L^{(2)}(z_1,z_3)\odot\begin{pmatrix}\Delta\overrightarrow{G}\\ \odot\\ K^{(3)}(z_1,z_2,z_3)\end{pmatrix}\odot L^{(2)}(z_2,z_3). \tag{C13}$$

Putting Eqs. (10), (C1), and (C13) together, we get Eq. (C8).

The proof of Eq. (C8) is quite suggestive and it can be deduced that any of the Ward-type identities defined in Eq. (14) can be proved in a very similar way.

APPENDIX D: DERIVATION OF CPA-NVC FROM THE Σ-DERIVABLE CPA THEORY

The central quantity to study in CPA-NVC [13,20] is the correlator (repeated indices are to be integrated out)

$$\langle\mathcal{G}(11')C(1'2)\mathcal{G}(22')\rangle\equiv L^{(2)}(11'22')C(1'2), \tag{D1}$$

where C can be any disorder-independent quantity. Note that we are using the collective index which consists of a space-time variable plus a Keldysh component. Following the same logic leading to Eqs. (C2) and (C3), we rewrite the quantity (D1) as

$$L^{(2)}(11'22')C(1'2)=G(11')[C(1'2)+\Lambda(1'2)]G(22'), \tag{D2}$$

where the vertex correction Λ satisfies

$$\Lambda(1'2)=K^{(2)}(1'\bar{1}\bar{2}2)G(\bar{1}\bar{3})[C(\bar{3}\bar{4})+\Lambda(\bar{3}\bar{4})]G(\bar{4}\bar{2})$$
$$=K^{(2)}\odot\begin{pmatrix}\overrightarrow{G}\\ \bullet\\ \overleftarrow{G}\end{pmatrix}\odot C+K^{(2)}\odot\begin{pmatrix}\overrightarrow{G}\\ \bullet\\ \overleftarrow{G}\end{pmatrix}\odot\Lambda$$
$$=K^{(2)}\odot L^{(2)}\odot C, \tag{D3}$$

where in the last equality Eq. (D2) has been used. As the CPA kernels are purely local in space, the vertex correction Λ can be decomposed as

$$\Lambda=\sum\nolimits_i\Lambda_i=\sum\nolimits_i K^{(2)}_i\odot\Theta_i, \tag{D4}$$

where Θ_i denotes the spatially diagonal part of the quantity (D1), i.e.,

$$\Theta_i\equiv\langle\mathcal{G}(11')C(1'2)\mathcal{G}(22')\rangle_i. \tag{D5}$$

Inserting a unit matrix $1\bullet 1$ in between $K^{(2)}_i$ and Θ_i, we get from Eq. (D4)

$$\Lambda_i=K^{(2)}_i\odot\begin{pmatrix}\overrightarrow{G}_{ii}\\ \bullet\\ \overleftarrow{G}_{ii}\end{pmatrix}\odot\begin{pmatrix}\overrightarrow{G}^{-1}_{ii}\\ \bullet\\ \overleftarrow{G}^{-1}_{ii}\end{pmatrix}\odot\Theta_i, \tag{D6}$$

where G_{ii} is the local part of the medium Green's function. Multiplying both sides of Eq. (D6) by $L^{(2)}_i$ [defined in Eq. (20)] from left and then adding Θ_i, we arrive at

$$\Theta_i+L^{(2)}_i\odot\Lambda_i=\left[L^{(2)}_i\odot K^{(2)}_i\odot\begin{pmatrix}\overrightarrow{G}_{ii}\\ \bullet\\ \overleftarrow{G}_{ii}\end{pmatrix}+\begin{pmatrix}\overrightarrow{G}_{ii}\\ \bullet\\ \overleftarrow{G}_{ii}\end{pmatrix}\right]$$
$$\odot\begin{pmatrix}\overrightarrow{G}^{-1}_{ii}\\ \bullet\\ \overleftarrow{G}^{-1}_{ii}\end{pmatrix}\odot\Theta_i. \tag{D7}$$

As $K^{(2)}_i$ is the exact kernel for $L^{(2)}_i$ within the local SIAM problem (see Sec. II C), the quantity in the above square brackets can be replaced with $L^{(2)}_i$ by means of Bethe-Salpeter equation [46]. Then, by rearrangement Eq. (D7) becomes

$$\Theta_i=L^{(2)}_i\odot\left[\begin{pmatrix}\overrightarrow{G}^{-1}_{ii}\\ \bullet\\ \overleftarrow{G}^{-1}_{ii}\end{pmatrix}\odot\Theta_i-\Lambda_i\right].$$

Using the explicit expression of $L^{(2)}_i$ [see Eq. (20)], we get

$$\Theta_i=\int dv_i\,p(v_i)\,g_{v_i}[(G_{ii})^{-1}\Theta_i(G_{ii})^{-1}-\Lambda_i]g_{v_i}, \tag{D8}$$

where all the quantities should be understood as 2×2 matrices in the Keldysh space [8,20]. To make connection with the CPA-NVC theory we shall utilize the multiple-scattering t matrix, which is related to G_{ii} and g_{v_i} via [20,27,28]

$$g_{v_i}=G_{ii}(1+t_iG_{ii}). \tag{D9}$$

Note that t_i is also a 2×2 Keldysh matrix and that it depends on the random potential v_i. An important result from CPA is that the average t matrix vanishes [20,24,27,28], namely

$$\langle t_i\rangle_{v_i}\equiv\int dv_i\,p(v_i)t_i=0. \tag{D10}$$

Substituting Eq. (D9) into Eq. (D8) and employing Eq. (D10), we get

$$\Lambda_i=\langle t_i\Theta_it_i\rangle_{v_i}-\langle t_iG_{ii}\Lambda_iG_{ii}t_i\rangle_{v_i}.$$

Finally, using Eqs. (D1), (D2), and (D5), we derive the NVC formula [13,20]

$$\Lambda_i=\langle t_i(GCG)_{ii}t_i\rangle_{v_i}+\sum_{j\neq i}\langle t_iG_{ij}\Lambda_jG_{ji}t_i\rangle_{v_i}. \tag{D11}$$

At this point, it is worth stressing again that all the quantities in the above formula should be understood as Keldysh matrices. Therefore, Eq. (D11) serves as a unified recursive relation for vertex corrections of all types of $L^{(2)}$ correlators [20].

[1] International Technology Roadmap for Semiconductors, http://www.itrs.net.

[2] S. Datta, *Electronic Transport in Mesoscopic Systems* (Cambridge University Press, Cambridge, UK, 1997).

[3] H. Haug, A.-P. Jauho, and M. Cardona, *Quantum Kinetics in Transport and Optics of Semiconductors* (Springer, Berlin, 2008), Vol. 2.

[4] A. Asenov, IEEE Trans. Electron Devices **45**, 2505 (1998).

[5] Y. Zhu, L. Liu, and H. Guo, Phys. Rev. B **88**, 085420 (2013).

[6] T. Markussen, R. Rurali, A.-P. Jauho, and M. Brandbyge, Phys. Rev. Lett. **99**, 076803 (2007).

[7] J. Taylor, H. Guo, and J. Wang, Phys. Rev. B **63**, 245407 (2001).

[8] J. Rammer, *Quantum Field Theory of Non-equilibrium States* (Cambridge University Press, Cambridge, UK, 2007).

[9] A. Kamenev, *Field Theory of Non-equilibrium Systems* (Cambridge University Press, Cambridge, UK, 2011).

[10] N. A. Sinitsyn, A. H. MacDonald, T. Jungwirth, V. K. Dugaev, and J. Sinova, Phys. Rev. B **75**, 045315 (2007).

[11] B. Velický, Phys. Rev. **184**, 614 (1969).

[12] G. Mahan, *Many-Particle Physics* (Plenum Press, New York, 1981).

[13] Y. Ke, K. Xia, and H. Guo, Phys. Rev. Lett. **100**, 166805 (2008).

[14] K. Levin, B. Velický, and H. Ehrenreich, Phys. Rev. B **2**, 1771 (1970).

[15] B. L. Altshuler, D. Khmel'nitzkii, A. I. Larkin, and P. A. Lee, Phys. Rev. B **22**, 5142 (1980).

[16] S. Feng, C. Kane, P. A. Lee, and A. D. Stone, Phys. Rev. Lett. **61**, 834 (1988).

[17] N. Zhu, H. Guo, and R. Harris, Phys. Rev. Lett. **77**, 1825 (1996).

[18] E. Akkermans and G. Montambaux, *Mesoscopic Physics of Electrons and Photons* (Cambridge University Press, Cambridge, UK, 2007).

[19] Q. Shi, H. Guo, Y. Zhu, and L. Liu, Phys. Rev. Appl. **3**, 064008 (2015).

[20] J. Yan and Y. Ke, Phys. Rev. B **94**, 045424 (2016).

[21] H.-K. Zhao and J. Wang, Phys. Rev. B **74**, 245401 (2006).

[22] Q.-F. Sun, J. Wang, and T.-H. Lin, Phys. Rev. B **61**, 13032 (2000).

[23] R. J. Elliott, J. A. Krumhansl, and P. L. Leath, Rev. Mod. Phys. **46**, 465 (1974).

[24] P. Soven, Phys. Rev. **156**, 809 (1967).

[25] D. W. Taylor, Phys. Rev. **156**, 1017 (1967).

[26] K. Carva, I. Turek, J. Kudrnovský, and O. Bengone, Phys. Rev. B **73**, 144421 (2006).

[27] Y. Zhu, L. Liu, and H. Guo, Phys. Rev. B **88**, 205415 (2013).

[28] A. V. Kalitsov, M. G. Chshiev, and J. P. Velev, Phys. Rev. B **85**, 235111 (2012).

[29] C. Zhou, X. Chen, and H. Guo, Phys. Rev. B **94**, 075426 (2016).

[30] I. Turek, V. Drchal, J. Kudrnovsky, M. Sob, and P. Weinberger, *Electronic Structure of Disordered Alloys, Surfaces, and Interfaces* (Springer Science & Business Media, New York, 2013).

[31] X. Jia, K. Xia, Y. Ke, and H. Guo, Phys. Rev. B **84**, 014401 (2011).

[32] Y. Ke, F. Zahid, V. Timoshevskii, K. Xia, D. Gall, and H. Guo, Phys. Rev. B **79**, 155406 (2009).

[33] Y. Ke, K. Xia, and H. Guo, Phys. Rev. Lett. **105**, 236801 (2010).

[34] D. Liu, X. Han, and H. Guo, Phys. Rev. B **85**, 245436 (2012).

[35] J. Maassen and H. Guo, Phys. Rev. Lett. **109**, 266803 (2012).

[36] G. Baym and L. P. Kadanoff, Phys. Rev. **124**, 287 (1961).

[37] G. Stefanucci and R. Van Leeuwen, *Nonequilibrium Many-Body Theory of Quantum Systems: A Modern Introduction* (Cambridge University Press, Cambridge, UK, 2013).

[38] J. W. Negele and H. Orland, *Quantum Many-Particle Systems*, Advanced Books Classical, Vol. 200 (Addison-Wesley, New York, 1988).

[39] A. Altland and B. D. Simons, *Condensed Matter Field Theory* (Cambridge University Press, Cambridge, UK, 2010).

[40] M. Jarrell and H. R. Krishnamurthy, Phys. Rev. B **63**, 125102 (2001).

[41] Note that Eq. (11) should be viewed as a formal expression only: When deriving $K^{(n+1)}$ from $K^{(n)}$, one removes Green's function lines from only one single edge of each $K^{(n)}$ diagram (see Fig. 2).

[42] G. Baym, Phys. Rev. **127**, 1391 (1962).

[43] D. Vollhardt and P. Wölfle, Phys. Rev. B **22**, 4666 (1980).

[44] V. Janiš, J. Phys.: Condens. Matter **15**, L311 (2003).

[45] V. Janiš, Phys. Rev. B **64**, 115115 (2001).

[46] A. Georges, G. Kotliar, W. Krauth, and M. J. Rozenberg, Rev. Mod. Phys. **68**, 13 (1996).

[47] H. Aoki, N. Tsuji, M. Eckstein, M. Kollar, T. Oka, and P. Werner, Rev. Mod. Phys. **86**, 779 (2014).

[48] D. Vollhardt, in *Lectures on the Physics of Strongly Correlated Systems XIV: Fourteenth Training Course in the Physics of Strongly Correlated Systems*, AIP Conf. Proc., Vol. 1297 (AIP, Melville, NY, 2010), pp. 339–403.

[49] H. Terletska, S.-X. Yang, Z. Y. Meng, J. Moreno, and M. Jarrell, Phys. Rev. B **87**, 134208 (2013).

[50] A. Gonis, *Green Functions for Ordered and Disordered Systems* (North-Holland, New York, 1992).

[51] V. Janiš and D. Vollhardt, Phys. Rev. B **63**, 125112 (2001).

[52] V. Janiš and V. Pokorný, Phys. Rev. B **81**, 165103 (2010).

[53] B. Sachs, T. O. Wehling, M. I. Katsnelson, and A. I. Lichtenstein, Phys. Rev. B **94**, 224105 (2016).

[54] T. G. Pedersen and J. G. Pedersen, Phys. Rev. B **87**, 155433 (2013).

[55] J. Wang, J. Comput. Electron. **12**, 343 (2013).

[56] B. Wang, J. Wang, and H. Guo, Phys. Rev. Lett. **82**, 398 (1999).

[57] M. P. Anantram and S. Datta, Phys. Rev. B **51**, 7632 (1995).

[58] T. Yamamoto, K. Sasaoka, S. Watanabe, and K. Watanabe, Phys. Rev. B **81**, 115448 (2010).

[59] Y. He, D. Hou, X. Liu, C. Fan, and R. Han, J. Phys.: Condens. Matter **18**, 8707 (2006).

[60] Y. He, R. Han, and H. Q. Xu, J. Phys.: Conf. Ser. **100**, 052065 (2008).

[61] Z. Chen, J. Zhang, and Z. Yu, in *IWCE'09: 13th International Workshop on Computational Electronics* (IEEE, Beijing, China, 2009), p. 1.

[62] S. Zhou, J. Jiang, and Q. Cai, J. Phys. D: Appl. Phys. **38**, 255 (2005).

[63] D. Kienle and F. Léonard, Phys. Rev. Lett. **103**, 026601 (2009).

[64] J. Wang, S. Liu, and Z. Chen, Phys. Lett. A **354**, 466 (2006).